Inorganic Chemistry
Cite This: Inorg. Chem. 2018, 57, 13397−13408
Article
pubs.acs.org/IC

Broad-Range Spectral Analysis for Chiral Metal Coordination Compounds: (Chiro)optical Superspectrum of Cobalt(II) Complexes

Gennaro Pescitelli,*[,†] Steffen Lüdeke,*[,‡] Anne-Christine Chamayou,[‡] Marija Marolt,[‡] Viktor Justus,[‡] Marcin Górecki,[†,§] Lorenzo Arrico,[†] Lorenzo Di Bari,[†] Mohammad Ariful Islam,[∥] Irina Gruber,[⊥] Mohammed Enamullah,*[,∥] and Christoph Janiak*[,⊥]

[†]Department of Chemistry and Industrial Chemistry, University of Pisa, 56126 Pisa, Italy
[‡]Institute of Pharmaceutical Sciences, University of Freiburg, D-79104 Freiburg, Germany
[§]Institute of Organic Chemistry, Polish Academy of Sciences, 01-224 Warsaw, Poland
[∥]Department of Chemistry, Jahangirnagar University, Dhaka-1342, Bangladesh
[⊥]Institute of Inorganic Chemistry and Structural Chemistry, University of Düsseldorf, D-40225 Düsseldorf, Germany

Supporting Information

ABSTRACT: Chiroptical broad-range spectral analysis extending from UV to mid-IR was employed to study a family of Co(II) *N*-(1-(aryl)ethyl)salicylaldiminato Schiff base complexes with pseudotetrahedral geometry associated with chirality-at-metal of the Δ/Λ type. While common chiral organic compounds have well-separated absorption and circular dichroism spectra (CD) in the UV/vis and IR regions, chiral Co(II) complexes feature an almost unique continuum of absorption and CD bands, which cover in sequence the UV, visible, near-IR (NIR), and IR regions of the electromagnetic spectrum. They can be collected in a single (chiro)optical superspectrum ranging from the UV (230 nm, 5.4 eV) to the mid-IR (1000 cm^{-1}, 0.12 eV), which offers a fingerprint of the structure and stereochemistry of the metal complexes. Each region of the superspectrum contributes to one piece of information: the NIR-CD region, in combination with TDDFT calculations, allows a reliable assignment of the metal-centered chirality; the UV-CD region facilitates the analysis of the Δ/Λ diastereomeric equilibrium in solution; and the IR-VCD region contains a combination of low-lying metal-centered electronic states (LLES) and ligand-centered vibrations and displays characteristically enhanced and monosignate VCD bands. Circular dichroism in the NIR and IR regions is crucial to reveal the presence of d−d transitions of the Co(II) core which, due to the electric-dipole forbidden character, would be otherwise overlooked in the corresponding absorption spectra.

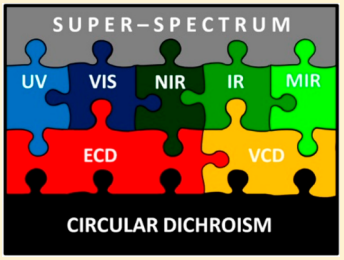

INTRODUCTION

The coordination chemistry of transition metals is rich of examples and applications of chirality.[1,2] Particularly interesting are those metal complexes where the metal itself is a center of chirality.[3−7] The stereochemistry of coordination compounds is in general quite sophisticated, because of the variable number of oxidation and valence states and different coordination geometries. However, if one is able to control all these aspects, coordination chemistry becomes a formidable tool for achieving elaborate chiral architectures with specific functions.[8−11] In addition to standard characterization techniques, chiral compounds can be investigated by means of chiroptical spectroscopies such as electronic and vibrational circular dichroism (ECD and VCD).[12,13] In the field of chiroptical spectroscopies, chiral coordination compounds are often much more than just chiral species containing one or more metal centers. In fact, they exhibit amazing properties associated with their metal core, for example plasmonic CD,[14,15] circularly polarized emission (CPL),[16,17] and magnetic circular dichroism.[18] Very recently, chiral Co(II) complexes have drawn new attention because of their capability of enhancing VCD signals of bound ligands.[19] VCD spectra contain a lot of structural information, but they suffer from intrinsically weak signal intensity (at least 2 orders of magnitude less than ECD).[20] Therefore, the phenomenon of VCD enhancement is of great interest for sensing purposes.[21−25] In addition to—and related to—enhanced VCD signals, Co(II) and other paramagnetic metal complexes manifest electronic transitions in the visible, the near-IR range, and even the IR range below 4000 cm^{-1}, which are also associated with significant CD signals. In fact, while almost all chiral organic compounds have distinctive and well separated IR/VCD and UV/ECD spectra, chiral Co(II) complexes feature an almost unique continuum of absorption and CD bands from the UV to the IR.

In this paper, we conceive a broad-range spectral analysis by assembling a (chiro)optical superspectrum composed of a continuous set of optical and chiroptical (CD) spectra, covering the whole range from 0.1 to 5.6 eV, that is, from the mid-IR through the NIR to the UV. To demonstrate the usefulness of this tool, we synthesized an array of enantiomeric *bis*{(*R* or *S*)-*N*-(1-(Ar)ethyl) salicylaldiminato} complexes of cobalt(II) with

Received: July 16, 2018
Published: October 19, 2018

Downloaded via DUESSELDORF LIBRARIES on November 7, 2018 at 10:23:50 (UTC).
See https://pubs.acs.org/sharingguidelines for options on how to legitimately share published articles.

© 2018 American Chemical Society

DOI: 10.1021/acs.inorgchem.8b01932
Inorg. Chem. 2018, 57, 13397−13408

different aryl groups {Ar = C_6H_5 (**1**), *p*-$MeOC_6H_4$ (**2**), *p*-ClC_6H_4 (**3**), and *p*-BrC_6H_4 (**4**), Scheme 1}. Of these, compound

Scheme 1. (a) Induced Chirality-at-Metal with Δ(right)- and Λ(left)-Handed Helicity in C2-Symmetrical Pseudotetrahedral Geometry.[a] (b) Structure of bis{(*R*/*S*)-*N*-(1-(Ar)ethyl) salicylaldiminato} Λ/Δ-cobalt(II) complexes 1−4.[b]

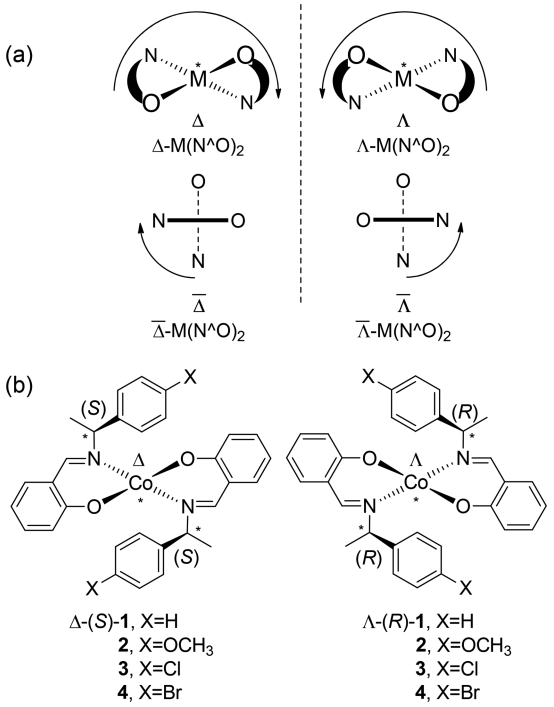

[a]The corresponding $\bar{\Delta}$ and $\bar{\Lambda}$ notation used for bis(bidentate) (pseudo)tetrahedral complexes is also illustrated. [b]For a given ligand configuration (*R* or *S*), only the dominant chirality-at-metal is shown (Λ and Δ, respectively).

(*R*)-**1** had been reported before.[26] The coordination of bidentate Schiff base ligands to divalent metal ions yields pseudotetrahedral complexes with metal-centered chirality.[27−33] In the case of bis(bidentate) tetrahedral or quasi-tetrahedral complexes of $M(A^{\wedge}B)_2$ type, the chirality-at-metal is designated by means of the $\bar{\Delta}/\bar{\Lambda}$ notation summarized in Scheme 1;[34] henceforth, we will use the corresponding Δ/Λ symbols for simplicity and consistence with previous literature on analogous compounds.[27−33]

The (chiro)optical superspectra of the family of Co(II) complexes **1**−**4** feature a wide ensemble of electronic and vibrational transitions, offering a distinctive fingerprint of their structure and stereochemistry. The analysis of the superspectrum, interpreted by means of density functional theory (DFT) and time-dependent DFT (TDDFT) calculations, provided information on several aspects.

(1) The absolute configuration of the chiral metal centers, namely the chirality-at-metal, could be established by comparing the experimental and calculated superspectrum with special attention to NIR-ECD spectra. While this region is generally poorly exploited (except for lanthanide complexes),[35] for metal complexes with unpaired d-electrons such as Co(II) ones, it exhibits signals with high *g*-values characteristic for the coordination geometry.

(2) Variable temperature ECD spectra are diagnostic of the diastereomeric equilibrium between species with same ligand configuration [(*R*) or (*S*)], but variable Δ or Λ configuration at the metal. This phenomenon has been thoroughly studied for analogous configurationally labile compounds.[27−29] As the NMR analysis of many paramagnetic compounds is hampered by peak broadening, the CD intensities observed in the UV region could be used to quantitatively probe the Δ:Λ ratio. Moreover, different from NMR, ECD and VCD spectra also provide information on the absolute stereochemistry.[13]

(3) VCD spectra of compounds **1**−**4** display several unique aspects, including the presence of broad bands in the 2300−3000 cm^{-1} region due to low-lying electronic excitations, and the enhancement of several VCD peaks in the mid-IR region with a dominant sign for a given configuration. According to current VCD theories, the two phenomena are strictly related to each other.[19,20,36]

The use of a (chiro)optical superspectrum tool emphasizes how Co(II) compounds feature a continuous series of electronic and vibrational transitions from ultraviolet to mid-IR (≈0.1−5.6 eV), virtually without interruptions. In this way, the complex electronic structure of Co(II) compounds is manifest, offering a new perspective in the structural analysis of chiral Co(II) species, which include for instance powerful enantioselective catalysts,[37,38] metal−organic frameworks[39] and cobalt proteins.[40] Moreover, the superspectra make the spectral similarities within a family of compounds easily appreciable. This is beneficial for several other classes of compounds, for example lanthanide complexes,[41] for which the isostructurality along the lanthanide series is an important issue.[42] Finally, the broad-band chiroptical analysis turns out to be particularly significant in the analysis of those phenomena, like the VCD enhancement, which depend in a specific way on the communication between ground-state vibrations and electronic excited states.

RESULTS AND DISCUSSION

Synthesis and Characterization. The synthesis of cobalt(II) complexes **1**−**4** was achieved by employing a previously reported procedure (Scheme S-A1, Supporting Information).[27−33] The enantiopure Schiff base ligands reacted with cobalt(II) acetate or sulfate in the presence of $NaHCO_3$ or NEt_3 under reflux, respectively, to provide compounds **1**−**4** (for details see Materials and Methods and Supporting Information). IR spectra of **1**−**4** show the main characteristic band at 1620−1600 cm^{-1} for the $\nu_{C=N}$ stretching vibration. EI-mass spectra show the parent ion peak ($[M]^+$) at *m*/*z* 507 (**1**), 567 (**2**), and 665 (**4**) and several ion peaks for fragmented species for both the complexes and ligands (see Section S-A2 in the Supporting Information). NMR spectra of **1**−**4** are dominated by shifting and peak broadening effects due to the paramagnetic Co(II) core. This prevents the use of NMR signals to quantify the Δ/Λ equilibrium (the method used for the Zn homoleptic series).[27]

Complex **2** was further characterized by cyclic voltammetry (CV), and complexes **1**, **2**, and **4** by differential scanning calorimetry (DSC). The experiments and results are summarized in the Supporting Information (Sections S-A3 and S-A4).

Crystallography. Crystals suitable for X-ray analysis were collected for all compounds **1**−**4**. The Co(II) atoms have a four-coordinated structure, in line with the d^7-configuration of Co(II) and the weak-field ligand character. The two N,O-

DOI: 10.1021/acs.inorgchem.8b01932
Inorg. Chem. 2018, 57, 13397−13408

bidentate Schiff base ligands form a near-tetrahedral and only slightly distorted N_2O_2-coordination sphere around the metal atom (Figure 1). In the solid state complete diastereoselectivity

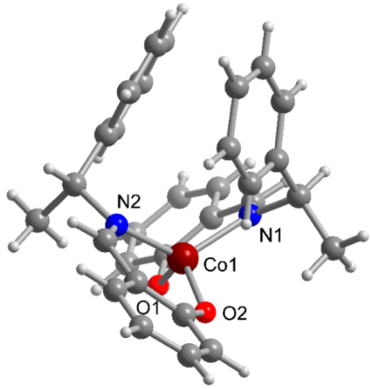

Figure 1. X-ray molecular structure of Λ-(*R*)-**1** emphasizing the quasi-tetrahedral N_2O_2-coordination sphere. See Figure S-B1 in the Supporting Information for the packing diagram and Table S-B2 for bond lengths and angles.

is found, such that the metal-centered configuration in the complexes prepared from enantiopure (*R*) or (*S*) ligands is uniquely Λ or Δ, respectively. This is in agreement with a previous assignment[26] of the configuration of compound (*R*)-**1** based on the isomorphism of its crystal structure with the homoleptic Zn complex.[43] It should be noted that the configuration observed in the crystal structure is not necessarily retained in solution.[28] The molecular structures for the Λ-(*R*) and Δ-(*S*) enantiomorphic pairs of compounds **1**−**4**, the packing diagrams, structural data, and additional discussion on the tetrahedral distortion are reported in the Supporting Information.

Magnetic Measurements. Magnetic moment and magnetic susceptibility were measured in methanol with the Evans' NMR method[44−47] for **1**, over a temperature range of 210−305 K, using one cooling and one heating scan (see details in Section S-A5, Supporting Information). The changes of magnetic susceptibility (χ) and magnetic moments (μ_{eff}) with the temperature are shown in Figure 2; μ_{eff} ranges between 4.0

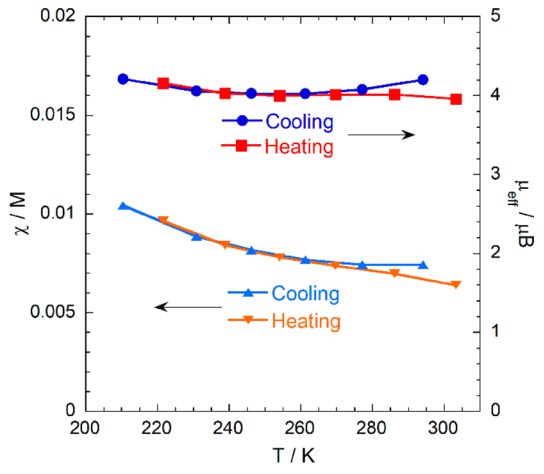

Figure 2. Changes of magnetic susceptibilities (χ) and magnetic moments (μ_{eff}) values with temperature for (*R*)-**1** (0.868 mM in methanol).

and 4.2 μ_B. The reproducibility of data for the cooling and heating curves excludes any decomposition or structural changes (i.e., no change of spin state) of the complex over the investigated temperature range in solution. The magnetic moment of **3** was measured in the solid state with a magnetic balance at room temperature and amounted to 4.2 μ_B.

The observed magnetic moments values (μ_{eff} = 4.0−4.2 μ_B for both compounds) correspond to the existence of a tetrahedral high-spin cobalt(II) complex.[48−50] The spin magnetic moment for three unpaired electrons is 3.88 μ_B; the residual difference (0.1−0.3 μ_B) with respect to the measured value of μ_{eff} is due to the contribution of the orbital angular magnetic moment.[51]

Chiro(optical) Superspectra: Experiments. The family of high-spin Co(II) complexes **1**−**4** offers a unique platform to investigate the entire electromagnetic spectrum from 0.1 to 5.6 eV by means of optical spectroscopies, namely UV/vis, near-IR (NIR), and mid-IR, and their chiroptical counterparts ECD, NIR-CD, and VCD. Routinely, UV/vis (ECD) and IR (VCD) spectra are displayed separately, because the intermediate NIR range hardly provides spectral information. However, Co(II) complexes show a continuous pattern of transitions from the UV to the mid-IR. In particular, various absorption and circular dichroism bands can be detected in the Vis and NIR regions, and broad bands due to low-lying electronic transitions appear in the IR between 2000 and 3200 cm^{-1} (0.25−0.4 eV), superimposed with narrow vibrational bands. Therefore, we envisaged that a continuous (chiro)optical "superspectrum" covering the whole 0.1−6 eV range would provide a distinctive fingerprint of the present complexes. Optical and chiroptical superspectra are shown in Figures 3 and 4 for compounds **1** and **3**, and in the Supporting Information for compounds **2** and **4** (Figure S-C1 and S-C2). In these spectra, we use the typical wavelength (in nm) and wavenumber units (in cm^{-1}) for the UV/vis−NIR and IR regions, respectively; however, eV values are also displayed on the top *x* axis as a common energy reference.

At first glance, inspection of the superspectra reveals the following points:

(1) The absorption spectra are identical for the two enantiomers of each compound, while CD spectra are the mirror image of each other, as expected.

(2) The overall spectral profile is very similar along the series in all the covered spectral regions; the only exception is the mid-IR (fingerprint) region, where VCD spectra allow a clear distinction among derivatives with different *para*-phenyl substitution.

(3) The signs of the chiroptical spectra are completely consistent for the same ligand absolute configuration, so that this latter is immediately reported by ECD and VCD spectra; VCD spectra are largely monosignate (negative for the *R* configuration) instead of exhibiting bands with alternating sign as commonly found. Moreover, they have enhanced intensity in comparison to free ligands and homoleptic Zn or Cu complexes.[27,28]

We shall now analyze the various regions in detail.

UV region (230−450 nm). In the UV region, pseudotetrahedral salicylaldiminato-metal complexes exhibit characteristic absorption and ECD spectra due to the $\pi-\pi^*$ transitions of the ligand aromatic chromophores.[27,28,31,52] Occurrence of exciton coupling is expected in such a situation where two chromophoric ligands are held together in a more or less fixed orientation around a metal core.[53] However, the effective observation of ECD exciton couplets (i.e., two bands with

DOI: 10.1021/acs.inorgchem.8b01932
Inorg. Chem. 2018, 57, 13397−13408

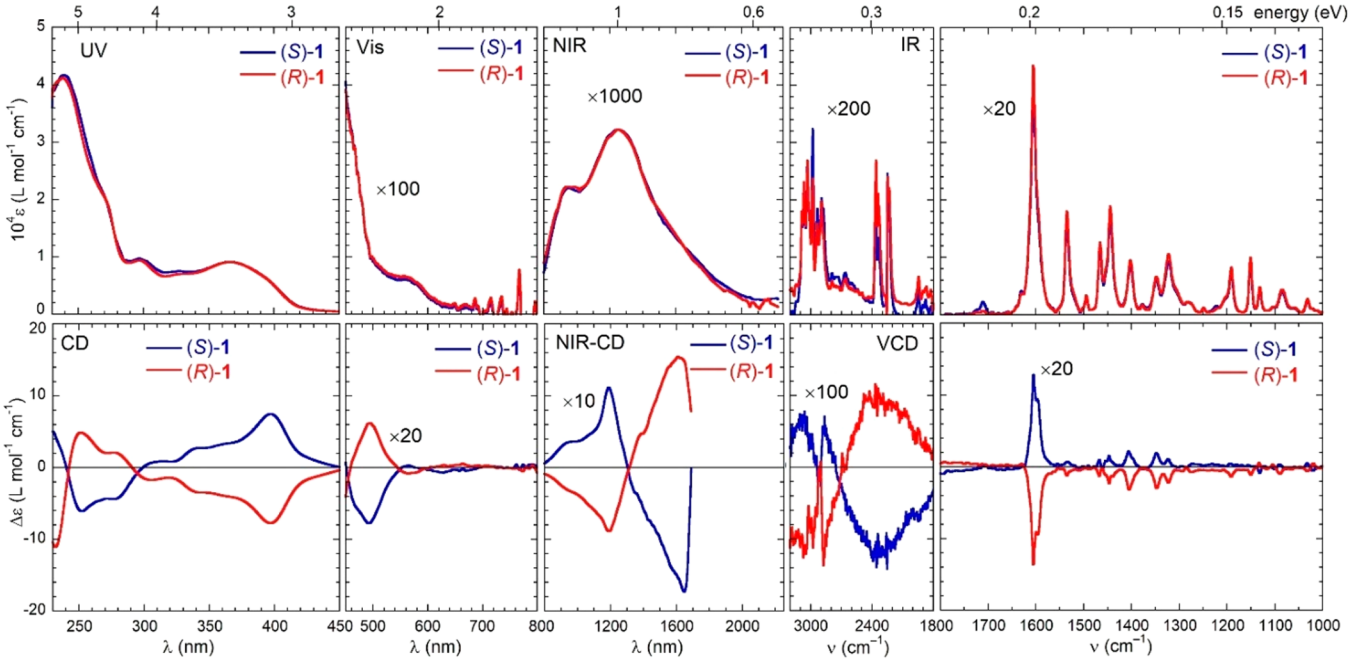

Figure 3. Optical (top) and chiroptical (bottom) superspectrum of (*R*)-**1** (red curves) and (*S*)-**1** (blue curves). See Materials and Methods for conditions.

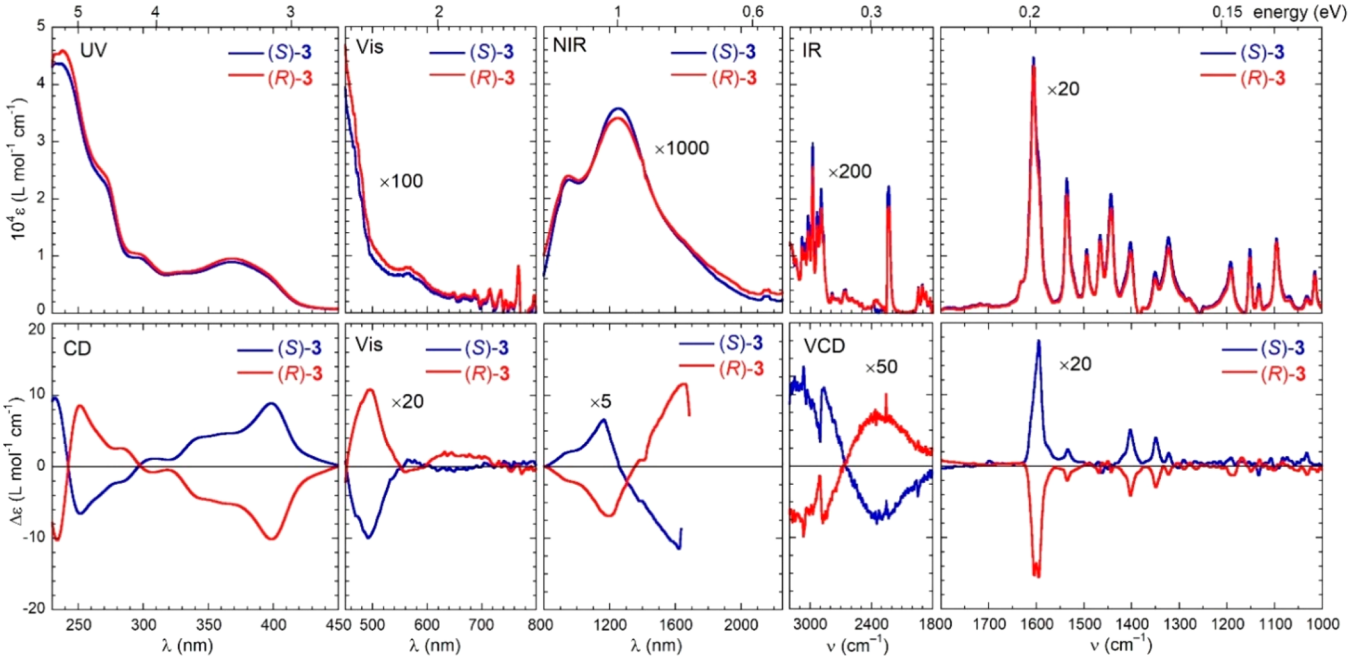

Figure 4. Optical (top) and chiroptical (bottom) superspectrum of (*R*)-**3** (red curves) and (*S*)-**3** (blue curves). See Materials and Methods for conditions.

opposite sign, similar intensity, and close wavelength maxima) depends on the mutual ligand orientation. In fact, bis-(salicylaldiminato) complexes of Ni(II) and Zn(II) behave differently in that respect because of the different coordination geometry.[54] The appearance of an ECD exciton couplet has been reported before in the so-called azomethine $\pi-\pi^*$ transition region (330−400 nm)[54] for compound (*R*)-**1** and analogous Zn(II) and Cu(II) species.[52] In our spectra, however, no clear-cut ECD exciton couplet exists in this region. Instead, compounds **1**−**4** feature an intense ECD band at 300−450 nm and a second one at 240−300 nm, which are for the *R*-configuration negative and positive, respectively. Both bands are very broad, well separated in energy and show one or more shoulders, witnessing the presence of several distinct transitions in this region, and can therefore hardly be interpreted in terms of exciton coupling.[53] The *g*-factor ($\Delta\varepsilon/\varepsilon$) in the UV range is around 2×10^{-4} for the short wavelength band, and 10^{-3} for the long wavelength band. Since the reciprocal arrangement between the aromatic chromophores is mainly dictated by the chirality-at-metal, the sign of ECD bands is indicative of the Δ/Λ-configuration but depends also on the ligand field geometry. In fact, the ECD spectra of the homoleptic series of Co(II),

DOI: 10.1021/acs.inorgchem.8b01932
Inorg. Chem. 2018, 57, 13397−13408

Zn(II), and Cu(II) are at large variance with each other, as demonstrated by Figure S-C5 (Supporting Information) for (*R*)-**3** and its Zn and Cu analogs.[27,28] Some similarity may be observed between the ECD spectra of the Co(II) and Zn(II) series, due to the related pseudotetrahedral geometry. For both metals, (*R*)-configured complexes exhibit dominant negative ECD above 300 nm (Figure S-C5, Supporting Information). For the homoleptic Zn(II) series, the leading diastereomers in solution were established to be (*R*)-Λ and (*S*)-Δ by means of VCD calculations and other evidence.[27] Thus, dominant negative ECD signals above 300 nm are a signature of complexes with Λ chirality-at-metal. Based on the consistency between the homoleptic Co(II) and Zn(II) series in terms of solid-state geometry and ECD spectra, we can infer from these analogies that all (*R*)-**1**−**4** complexes preferentially have dominant Λ chirality-at-metal in solution and that all (*S*)-**1**−**4** complexes have Δ chirality-at-metal. This is confirmed by DFT and TDDFT calculations (see below).

Variable temperature ECD measurements (VT-ECD) are a useful tool for investigating equilibria between distinct chemical species, such as the present diastereomeric Δ/Λ pair. VT-ECD spectra of (*R*)- and (*S*)-**3** were measured in acetone and showed a small but detectable temperature dependence; an isodichroic point at 397 nm became obvious when the difference ECD were plotted (Figure 5). These changes can be rationalized by

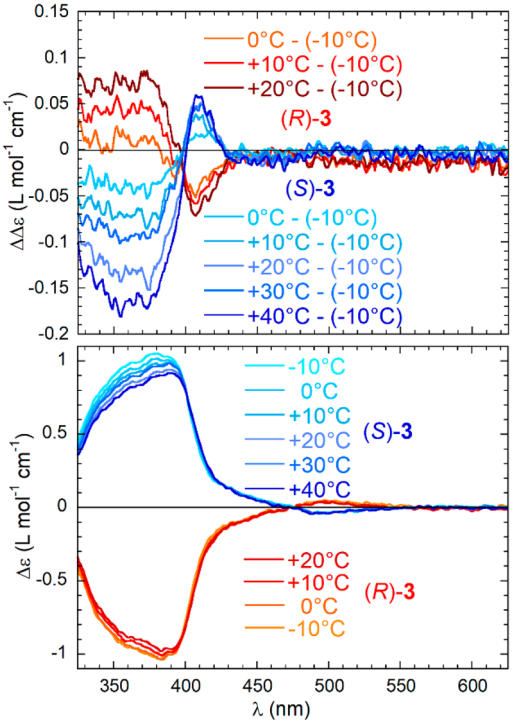

Figure 5. Bottom: ECD spectra of (*R*)- and (*S*)-**3** at different temperatures. The CD intensity at 380 nm shows a small decrease with increasing temperature. Top: difference spectra (with reference to −10 °C spectrum).

considering that the Δ and Λ-configured complexes are associated with ECD bands of opposite sign in this region. Thus, the fact that the lowest temperature (−10 °C) yields the strongest signal is consistent with the largest diastereomeric ratio (dr). Although the number of collected points is too low for an accurate determination, Boltzmann-fitting of the CD intensities at 380 nm suggests a free energy difference between the diastereomers of roughly 0.8 kcal/mol (see Supporting Information, Figure S−C3), meaning a dr ≈ 80:20 for Λ-Co-(*R*) vs Δ-Co-(*R*) at 300 K. We note that the NMR analysis of the homoleptic Zn(II) complexes in $CDCl_3$ solution afforded a virtually identical result with dr ≈ 80:20 for Λ-Zn-(*R*) vs Δ-Zn-(*R*) at room temperature.[27]

Summarizing, the analysis of UV-CD spectra provided a first hint of the dominant chirality-at-metal and made it possible to quantify of the Δ/Λ diastereomeric equilibrium in solution.

Vis Region (450−700 nm). In the Vis region, d^7 tetrahedral Co(II) complexes exhibit a set of d-d transitions, typical of transition metals with unpaired d electrons. For a d^7 Co(II) system with tetrahedral symmetry, a triply degenerate $^4A_2 \rightarrow {}^4T_1(P)$ transition occurs around 550 nm,[55] which is split into two or three components when the ideal symmetry is reduced to a lower one.[56,57] As we shall see below, however, this range includes transitions with considerable contributions from the ligand. The dominant Vis-ECD band is centered at 500 nm, it has a consistently positive sign for all compounds **1**−**4** with (*R*)-configuration, and attains *g*-values in the range $3-5 \times 10^{-3}$.

NIR Region (800−1700 nm). In the NIR region, all compounds show two ECD bands of alternating sign; for *R*-ligands, with a preferential Λ chirality-at-metal, a negative band centered around 1200 nm and a positive one centered around 1600 nm are consistently found. For a tetrahedral d^7 Co(II) system, a triply degenerate $^4A_2 \rightarrow {}^4T_1(F)$ transition is expected in the NIR, which is split by lowering symmetry.[55−57] These are mainly d-d transitions, allied with large magnetic and small electric transition moments. In fact, the ECD bands are relatively weak ($\Delta\varepsilon_{max}$ below 2 M^{-1} cm^{-1}), but the corresponding *g*-values are very large (up to 6×10^{-2} for the 1200 nm band and 3×10^{-1} for the 1600 nm band). This is a remarkably large value even for magnetic-dipole allowed d−d transitions of chiral metal complexes.[12] The fact that the shape and intensity of the NIR-CD signals are well preserved for the series **1**−**4** demonstrates that these bands sense especially the nearest ligand field of N/O atoms, whose geometry is similar for the various compounds.

In conclusion, the NIR-CD is immediately diagnostic of the chirality-at-metal and, in association with the very large *g*-values, makes this region especially useful for sensing purposes. As we shall see below, the NIR-CD signals are well reproduced by calculations, allowing a safe assignment of the Δ or Λ chirality-at-metal.

IR Region (800−3000 cm^{-1}). For several reasons, the IR region is the most peculiar one in our superspectra: (1) the mid-IR VCD spectra are almost monosignate being dominated by negative bands for *R* ligands and positive bands for *S* ligands; (2) the VCD signal is sizably enhanced in comparison to the VCD spectra of the free ligands or the homoleptic Zn and Cu complexes; (3) broad bands exist between 2000 and 3000 cm^{-1}, due to electronic transitions which overlap with vibrational ones. All these peculiarities are due to the high-spin d^7 Co(II) core, with its characteristic optical and magnetic properties. It is known that transition metal complexes with unpaired d-electrons may exhibit VCD signals enhanced by one or two orders of magnitude in comparison to the spectra of the homoleptic diamagnetic complexes.[19,20,36,58−64] This phenomenon has been attributed to the vibronic coupling between ground-state vibrational transitions and magnetic-dipole allowed low-lying electronic excited states (LLES).[19,20,36,65] Tetrahedral d^7 Co(II) systems feature a triply degenerate band of $^4A_2 \rightarrow {}^4T_2$ nature between 2000 and 7000 cm^{-1},[55] which is split into two or three components upon symmetry lowering.[56]

DOI: 10.1021/acs.inorgchem.8b01932
Inorg. Chem. 2018, 57, 13397−13408

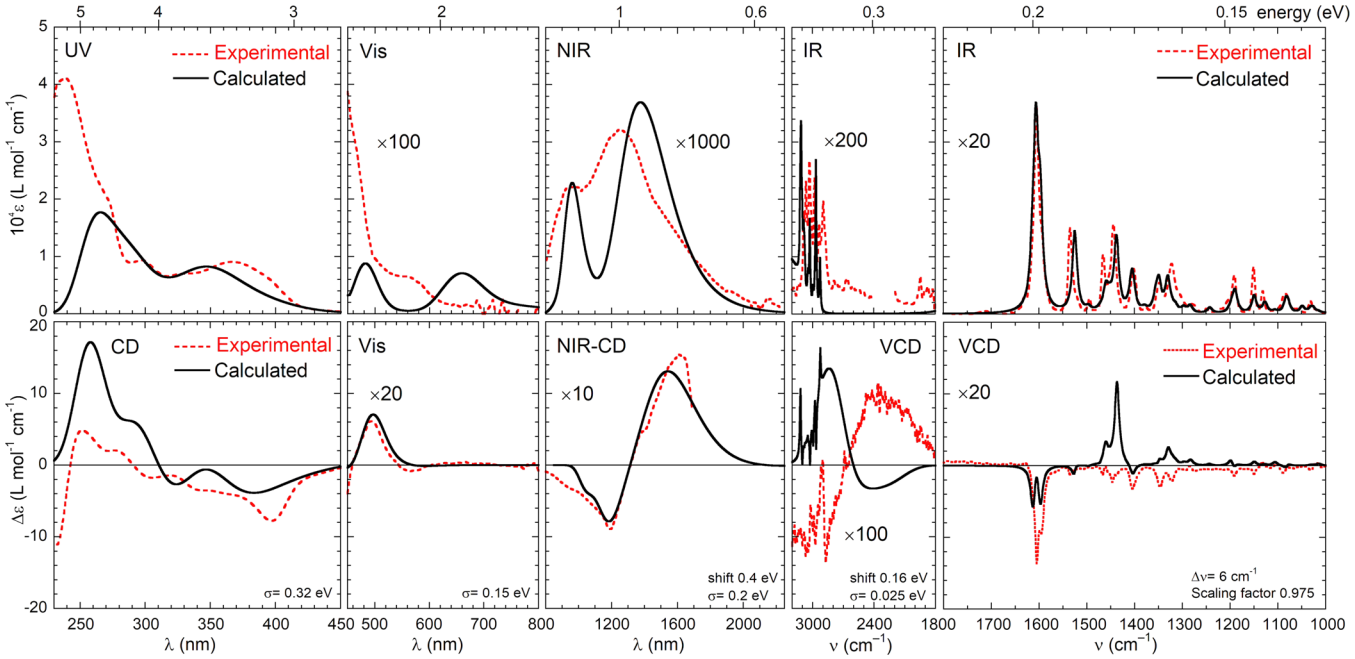

Figure 6. Calculated absorption (top) and CD superspectra (bottom) for (*R*)-**1** at the B3LYP/def2-TZVP level (solid black lines), compared with the absorption and CD experimental superspectra (dotted red lines). The parameters used to generate the calculated spectra in each region are given at the bottom of each section. TDDFT calculations were run at the B3LYP/def2-TZVP//M06-def2-SVP level and Boltzmann averaged over three Λ and four Δ conformers; DFT calculations were run at B3LYP/def2-TZVP level and Boltzmann averaged over two Λ conformers. In the high-frequency IR regions, TDDFT and DFT results were combined with each other using an arbitrary scaling factor.

Two broad bands of opposite signs appear for compounds **1**−**4** between 2000 and 3000 cm^{-1}, which are characteristically overlapped with the sharp C−H stretching modes. The dispersive appearance of these bands has been interpreted to be due to an interference mechanism between metal-centered d-d electronic transitions and ligand-centered C−H stretching vibrations.[58] Thus, a combination between the electric transition dipoles of ligand vibrations and the magnetic transition dipoles borrowed from metal d−d transitions may occur.

The VCD spectra of compounds **1**−**4** in the range 1000−1800 cm^{-1} (Figures 3−4 and S−C1−2, Supporting Information) are rather strong, with $\Delta\varepsilon$ values extending to 1 M^{-1} cm^{-1} for the C═N stretching vibrations around 1600 cm^{-1}, and corresponding *g*-values of up to 5 × 10^{-4}. VCD spectra of diamagnetic species hardly exceed *g*-values of 10^{-4}; for example, the homoleptic Zn complexes have $\Delta\varepsilon \approx 0.15$ M^{-1} cm^{-1} and $g \approx 6 \times 10^{-5}$ for the C═N stretching vibrations (Figure S−C4, Supporting Information).[27] The VCD spectra of the free salicylaldimine ligands are also very weak (data not shown). Thus, Co(II) complexes **1**−**4** display at least 10-fold enhanced VCD spectra with respect to their diamagnetic reference. This enhancement is not exceptional if compared to other literature reports.[36,58−64] What is however largely unprecedented for Co(II) compounds is the peculiar appearance of the VCD spectra, where a dominant sign appears for a given configuration. For example, the signal for C═N stretching vibrations at 1605 cm^{-1} is monosignate and negative for all Co-*R* complexes, while in other pseudotetrahedral chiral-at-metal complexes it appears as a characteristic bisignate signal due to the coupled oscillator mechanism (see Figure S-C4, Supporting Information, for the Zn- and Cu-analogs of **3**).[27,28] This monosignate appearance of VCD spectra is related to the VCD enhancement and cannot be reproduced by DFT calculations.

In summary, the characteristic enhancement and peculiar appearance of IR-VCD signals are responsible for VCD spectra which, despite not being reproduced by calculations, unveil the communication between ground-state vibrations and electronic excited states typical of Co(II) complexes.

Chiro(optical) Superspectra: Calculations. Quantum-chemical calculations of ECD and VCD spectra are widely used for assigning the absolute configuration of organic and organometallic compounds.[66] Density functional theory (DFT) represents the computational method with the best cost/accuracy compromise; thus, DFT calculations of VCD spectra and time-dependent DFT (TDDFT) calculations of ECD spectra are nowadays very popular.[67] While the ligand absolute configuration was known for the present compounds, CD calculations could be profitably employed to assign the (dominant) configuration at the metal center and to interpret and rationalize the observed ECD and VCD spectra.[66] It must be stressed that quantum-mechanical calculations of high-spin Co(II) complexes,[68] and excited-state calculations of metal complexes in general, may be complicated by several factors.[67,69,70] In particular, open-shell systems suffer from spin contaminations and other pitfalls.[71] Moreover, TDDFT calculations are intrinsically poorly accurate for high-lying electronic transitions,[72] which necessarily come into play with multichromophoric systems. Still, by means of a proper choice of the calculation method, we were able to reproduce the (chiro)optical superspectrum of the present compounds reasonably well on the whole range, except for the VCD spectrum. In fact, the theory accounting for LLES is not yet implemented in current theoretical models for DFT calculations of VCD spectra.[36]

Conformational Analysis. We focused on compound **1** and used the X-ray structure of Λ-(*R*)-**1** (Figure 1) as the starting geometry. Conformational searches with molecular mechanics

DOI: 10.1021/acs.inorgchem.8b01932
Inorg. Chem. 2018, 57, 13397−13408

and DFT geometry optimizations were run on the two possible diastereomers Λ-(*R*)-**1** and Δ-(*R*)-**1** to find the favored conformation. The details of our modeling approach are described in the Computational Section. All relevant structures obtained after DFT geometry optimizations are shown in the Supporting Information (Tables S-D1 and S-D2). The lowest-energy conformer found by M06/def2-SVP calculations has Λ-(*R*) configuration and resembles the X-ray geometry. The energy of the most stable conformer with Δ-(*R*) configuration is by 3.74 kcal/mol higher than the energy of the most stable conformer with Λ-(*R*) configuration (Table S-D1, Supporting Information). Inclusion of a solvent model (IEF-PCM) for chloroform did not affect substantially the relative energy of the various conformers (Table S-D1). Thus, M06/def2-SVP calculations predict correctly that the Λ-(*R*) diastereomer is the preferred one, although they overestimate the energy difference with the Δ-(*R*) diastereomer. In contrast, the use of the B3LYP functional led to an incorrect estimate of the relative stability of the two diastereomers. This shortcoming could be solved by applying a dispersion correction (D3BJ) to B3LYP,[73] by which the Λ-(*R*) form turned out to be the higher populated diastereomer (Table S-D2, Supporting Information).

Excited-State ECD Calculations. Because of the intrinsic difficulties of excited-state calculations of open-shell metal complexes mentioned above, the performance of several different combinations of DFT functionals and basis sets needed to be tested (see Computational Section) to check their ability to reproduce the portion of the superspectrum allied with electronic transitions (from UV to NIR).[68] The two best performing functionals were B3LYP[74,75] and M06-L,[76] while the use of def2-SVP or def2-TZVP basis sets[77] was similarly efficient. In Figure 6, the (chiro)optical superspectrum calculated on (*R*)-**1** at the B3LYP/def2-TZVP level is compared with the corresponding experimental superspectrum. The calculation results obtained at the M06-L/def2-TZVP[76] level are shown in Figure S-D1, while the results of other combinations of functionals and basis sets are summarized in Figure S-D2 (Supporting Information). The results obtained with the various functionals were relatively consistent with each other in the UV−vis region but much less in the NIR region, demonstrating the difficulty of TDDFT calculations on the present compounds.

There is an overall fair agreement between the experimental and calculated ECD superspectra of (*R*)-**1**, and the performance of calculations is remarkably good in the Vis and NIR regions (Figure 6). The series of two NIR-CD bands and a shoulder with +/−/− signs (from right to left) is correctly reproduced. As discussed above, this region is well preserved among the series and associated with the highest *g*-values, lending itself for a safe and sensitive stereochemical assignment. Based on these facts, TDDFT calculations allowed us to ultimately assign the stereochemistry of the dominant diastereomer of **1** as Λ-(*R*)-**1**. The sign of the two major NIR-CD bands (+/− from right to left) can then be taken as a signature of Λ chirality-at-metal for the entire series **1**−**4**.

The agreement between experimental and calculated spectra is less satisfactory in the UV region, where absorption and CD bands arise from several high-lying excitations (the number of roots was 80 for B3LYP and 120 for M06-L). Still, for the (*R*)-configuration, a dominant negative ECD sign is reproduced at longer wavelengths (300−450 nm for B3LYP, 360−470 nm for M06-L), and a dominant positive sign at shorter wavelengths (<300 nm for B3LYP, < 360 nm for M06-L), which is in line with the experimental observations (Figure 6). On the right edge of the electronic spectra (plotted in the 1800−3200 cm^{-1} panel) a bisignate ECD feature is predicted, though with opposite sign with respect to the experiment; in our calculations, this is due to the contribution of distinct conformers and is not related to electronic/vibrational interference effects. It must be stressed that the different sections of the calculated superspectrum were plotted with different band-widths and wavelength shifts (see values for σ, $\Delta\nu$ and shift in Figure 6). This latter expedient was necessary because the absolute transition energies are well reproduced by TDDFT calculations in the UV and Vis regions, but they are overestimated by 0.16−0.4 eV in the NIR and IR regions.[69] Anyway, a single density functional is not expected to simulate several transitions with very diverse characters equally well.[78] Moreover, because of the exceptional energy extension of the superspectrum, it would be unreasonable to apply the same bandwidth on the whole range. For example, 0.2 eV equals 24 nm at 400 nm and 670 nm at 2400 nm.

A second main result from ECD calculations is that the ECD spectra calculated separately for the two diastereomers Λ-(*R*)-**1** and Δ-(*R*)-**1** are almost exact mirror images of each other (Figure S-D3, Supporting Information). This finding is important for two reasons: (a) it demonstrates that the ECD spectrum is dominated by the chirality-at-metal, as found for other chiral bidentate Schiff bases complexes of various transition metals with pseudotetrahedral or pseudosquare -planar geometry;[27−32] (b) it makes it possible to assign the configuration at the metal center for the most stable diastereomer in solution, as we did above, especially looking at the NIR-CD signals.

Finally, additional information was provided by the analysis of electronic transitions and Kohn−Sham molecular orbitals (MO),[69] summarized in the Supporting Information (Figure S-D4). The frontier fully occupied and single-occupied MO are the five d orbitals of the Co(II) ion, as expected, mixed with p-type orbitals lying on the N/O ligand atoms. As it happens for other open-shell metal Schiff bases investigated before,[30−32] it is almost impossible to assign any calculated transition to a well-defined single excitation.[70,79] Even the first calculated transitions, which would in principle be assigned to "pure" d−d excitations, are heavily contaminated by the participation of ligand MO. This can be appreciated by looking at the transition density plots depicted in the Supporting Information (Figure S-D5), showing how the electron density is rearranged during each transition. The same picture witnesses the very high density of states in the UV region of the spectrum, which renders an accurate simulation of the ECD spectrum in this region especially difficult. Therefore, any simplified interpretation of ECD spectra for example in terms of exciton coupling[53,54] is not justified (see discussion in Section S-D1, Supporting Information).

Frequency (VCD-IR) Calculations. In the mid-IR region, the IR spectrum is well reproduced by DFT calculations, while the VCD counterpart is not (Figure 6, rightest panels). As said above, the theoretical model currently available for DFT calculations of VCD spectra does not fully include the vibronic coupling between ground-state vibrations and low-lying excited states (LLES).[36] This coupling is ultimately responsible for the VCD enhancement through the borrowing of the LLES magnetic-dipole term by the vibrational transitions.[19,20,65] It must be stressed that, in d^7 tetrahedral Co^{2+} complexes, the communication between the ground state and the first $^4T_2$ excited state is also provided by spin−orbit coupling. This is

DOI: 10.1021/acs.inorgchem.8b01932
Inorg. Chem. 2018, 57, 13397−13408

responsible for the non-negligible orbital magnetic moment (0.3−0.9 μ_B) observed for tetrahedral Co(II) halides $[CoX_4]^{2-}$ (X = Cl, Br),[80] which is in theory quenched for the $^4A_2$ ground-state.[51] The same is likely to happen for complexes **1**−**4**, yielding an orbital contribution to the static magnetic moment of ≈0.3 μ_B (as mentioned above).

Apart from underestimating the intensity of several VCD bands (especially between 1410 and 1480 cm^{-1} and 1300−1365 cm^{-1}, Figure 6), DFT calculations are not able to reproduce the fact that all experimental VCD bands are monosignate or at least heavily biased toward one sign (negative for (*R*)-**1**−**4**). A correlation between VCD enhancement and monosignate spectra (or specific spectral regions) has been noticed before for tris-chelated Co(III) complexes and interpreted through the first theory proposed for VCD enhancement, the ring-current theory.[63,81] Our finding demonstrates that such circumstance may also occur for Co(II) complexes and have broader implications on the VCD enhancement phenomenon.

CONCLUSIONS

We reported the synthesis and characterization of a family of chiral Co(II) *N*-[1-(aryl)ethyl]salicylaldiminato complexes **1**−**4** with variable aryl moieties. The crystal field geometry around the Co^{2+} core is pseudotetrahedral, and the complexes exhibit metal-centered Δ/Λ-chirality. Using enantiopure ligands, a complete diastereoselectivity is obtained in the solid state, where only Λ-(*R*) and Δ-(*S*) species are observed by X-ray crystallography. In solution, however, a diastereomeric equilibrium is detected, with a predominance of Λ-(*R*) and Δ-(*S*) species, respectively. The strong paramagnetism of the present high-spin Co(II) complexes **1**−**4** hampers the use of NMR spectroscopy in their characterization. On the other hand, the peculiar features of the high-spin d^7 Co^{2+} core open the way to using the tool of the (chiro)optical superspectrum. In fact, complexes **1**−**4** show a continuous distribution of electronic and vibrational transitions covering the electromagnetic spectrum from ultraviolet to mid-IR (≈0.1−5.6 eV), virtually without interruptions. Therefore, the (chiro)optical superspectrum offers a distinctive fingerprint of the structure and stereochemistry of the considered species. It allows the assignment of chirality-at-metal configuration (UV, Vis, NIR region), the ligand configuration (IR region), as well as the assessment of the Λ/Δ diastereomeric ratio. Especially remarkable is the near-IR region, where chiral Co(II) complexes exhibit CD bands with large *g*-values (up to 0.3), which are diagnostic of the chirality-at-metal. Moreover, in the mid-IR region between 2000 and 3000 cm^{-1}, there is a singular superposition of metal-centered electronic transitions and ligand-centered vibrational transitions. The resonance between electronic and vibrational transitions results in the enhancement of the VCD bands of paramagnetic complexes **1**−**4** reaching *g*-values one order of magnitude larger than those of the analogous Zn(II) and Cu(II) complexes. Additionally, the VCD spectra of homochiral complexes **1**−**4** are dominated by VCD bands of the same single sign. The fact that the mid-IR region is not predicted correctly by quantum chemical calculations underlines the importance of broad-range spectral analysis for studying open-shell chiral Co^{2+}-salicylaldiminato complexes: the evaluation of the vibrational part alone is prone to misinterpretations, as the theory that is currently implemented in quantum chemistry software packages does not accurately describe the vibronic coupling situation observed here. Still, the UV to NIR region allows a clear assignment of chirality-at-metal and the observation of the diastereomeric equilibrium.

Co(II) coordination compounds feature many remarkable examples which can be potentially analyzed by means of (chiro)optical superspectra.[37−40] However, the concept of the (chiro)optical superspectrum is not restricted to Co(II) compounds and may be extended to any chiral metal coordination complex featuring a manifold of electronic and vibrational transitions from the UV to the mid-IR,[59,82] also including emission spectra as a further dimension. Very promising candidates are chiral lanthanide complexes of Yb, Tm, Tb, Eu, and Sm,[41,64,83] especially in consideration of their applications in optoelectronic devices;[17] the existence of even lower lying excited states in these compounds gives rise to similar peculiar spectral features as observed in this study.

MATERIALS AND METHODS

See Supporting Information (Section S-A2) for the complete Materials and Methods. For variable temperature magnetic measurements by the Evans' method,[44−47] methanol was used in temperature calibration,[84] and dioxane in methanol (0.5%, v/v) as an internal reference compound (see details in Section S-A5, Supporting Information). Magnetic susceptibilities were measured at 298 K on solid samples with a Magway MSB Mk1 magnetic susceptibility balance (Sherwood Scientific Ltd.). Diamagnetic corrections were introduced according to König.[85]

(Chiro)optical Superspectra. *ECD and UV−Vis.* Spectra were recorded with a Jasco J−715 spectropolarimeter (Tokyo, Japan) in the range of 200−800 nm at room temperature in spectroscopic grade $CHCl_3$ (∼0.4 mM) in quartz cells with path length ranging from 0.1 cm (UV region) to 2 cm (Vis region). All spectra were measured using a scanning speed of 100 nm min^{-1}, a step size of 0.2 nm, a bandwidth of 2 nm, a response time of 0.5 s, and an accumulation of 4 or 8 scans. The spectra were background-corrected using spectra of $CHCl_3$ recorded under the same conditions. The spectrum of (*S*)-**1** showed traces of the free ligand, whose spectrum was then subtracted with the proper weight (ca. 0.2).

NIR-CD. Spectra were recorded with a Jasco J-200D spectropolarimeter (Tokyo, Japan) in the range of 800−1700 nm at room temperature in spectroscopic grade $CHCl_3$ (∼3 mM) in a quartz cell with a path length of 1 cm. All spectra were measured using a scanning speed of 50 nm min^{-1}, a step size of 0.2 nm, a bandwidth of 32 nm, a response time of 2 s, and an accumulation of 3 scans. The spectra were background-corrected using spectra of $CHCl_3$ recorded under the same conditions.

NIR Absorption. Spectra were recorded using a Jasco V-670 Spectrophotometer (Tokyo, Japan) in the range of 800−2700 nm at room temperature in spectroscopic grade $CDCl_3$ (∼3 mM) in a quartz cell with a path length of 2 cm. All spectra were measured using a scanning speed of 100 nm min^{-1}, a step size of 0.5 nm, a bandwidth of 8 nm, a fast response time, and an accumulation of 3 scans. The spectra were background-corrected using spectra of $CDCl_3$ recorded under the same conditions.

VCD and IR. Spectra at a resolution of 4 cm^{-1} were recorded for ∼40 mM solutions of **1**−**4** in $CDCl_3$ at room temperature using a Bruker Tensor 27 IR spectrometer equipped with a Bruker PMA 50 VCD sidebench module. All solutions were measured in a rotatable BaF_2 cell with a path length of 100 μm for 140 min (1800−950 cm^{-1}) or 200 min (3200−950 cm^{-1}). The optimum retardation value of the photoelastic modulator was set at 1400 cm^{-1} for 1800−950 cm^{-1} and at 2600 cm^{-1} for 3200−950 cm^{-1}. The spectra were averaged over all rotation angles and background-corrected using spectra of $CDCl_3$ recorded under the same conditions.

Synthetic Procedure. Enantiopure Schiff base ligands, (*R* or *S*)-*N*-(1-phenylethyl)salicylaldimine ($\mathbf{L_1}$) (225.2 mg, 1 mmol), were dissolved in 10 mL of methanol, and poured into 5 mL of a hot methanolic solution of $NaHCO_3$ (84 mg, 1 mmol). The solution mixture was stirred for 10 min. A solution of 124.5 mg (0.5 mmol) $Co(O_2CCH_3)_2{\cdot}4H_2O$ in 5 mL of methanol was added to the

DOI: 10.1021/acs.inorgchem.8b01932
Inorg. Chem. 2018, 57, 13397−13408

deprotonated Schiff base solution and refluxed for 4−5 h (ca. at 60 °C) under nitrogen atmosphere. Complexation was indicated by a color change from light-yellow to pink-red. Precipitates were filtered off, and the volume of the solution was reduced to *ca.* 50% in *vacuo*. This concentrated solution was left standing for crystallization via slow evaporation of the solvent at room temperature. The dark red (or pink-red) crystals of *bis*{(*R* or *S*)-(*N*-1-phenylethyl)salicylaldiminato}-cobalt(II) ((*R*)-**1** or (*S*)-**1**) (see Figure S-B5 in the Supporting Information), suitable for X-ray measurements, formed within 4−5 days. The crystals were separated and washed with methanol (2 mL, 2 times) and *n*-hexane (2 mL, 2 times) and were dried at 40 °C for 5−6 h. The same procedure was followed to synthesize the other *bis*{(*R* or *S*)-*N*-(1-(Ar)ethyl)salicylaldiminato}cobalt(II) complexes ((*R*)-**2** or (*S*)-**2** and (*R*)-**4** or (*S*)-**4**) using the respective Schiff bases (*R* or *S*)-*N*-(1-(Ar)ethyl)salicylaldimine {Ar = *p*-MeOC$_6$H$_4$ (**L$_2$**) and *p*-BrC$_6$H$_4$ (**L$_4$**)}. Experimental details and characterization data are reported in the Supporting Information (Section S-A2). Complexes **2**−**4** {(*R*)-**3** or (*S*)-**3**) with Ar = *p*-ClC$_6$H$_4$ (**L$_3$**)} were also prepared using an alternative procedure, as detailed in the Supporting Information.

Crystallography. Single crystals of enantiomeric pairs (*R*)/(*S*)-**1**, (*R*)/(*S*)-**2**,(*R*)/(*S*)-**3**, and (*R*)/(*S*)-**4** were carefully selected under a polarizing microscope and mounted on a loop. *Data collection*: Bruker APEX II CCD diffractometer with graphite-layer or multilayer mirror monochromated Mo Kα radiation (λ = 0.71073 Å); ω-scans (see Table S-B3, Supporting Information). Data collection and cell refinement with APEX2,[86] data reduction with SAINT (Bruker).[87] *Structure analysis and refinement:* The structures were solved by direct methods (SHELXS-97),[88] refinement was done by full-matrix least-squares on F^2 using the SHELXL-97 program suite, empirical (multiscan) absorption correction with SADABS (Bruker).[89] All non-hydrogen positions were refined with anisotropic temperature factors. Hydrogen atoms for aromatic and olefinic CH, aliphatic CH and CH_3 groups were positioned geometrically (C−H = 0.94 Å for aromatic and olefinic CH, 0.99 for aliphatic CH and 0.97 Å for CH_3,) and refined using a riding model (AFIX 43 for aromatic/olefinic CH, AFIX 13 for aliphatic CH, AFIX 137 for CH_3), with U_{iso}(H) = 1.2U_{eq}(CH) and U_{iso}(H) = 1.5U_{eq}(CH_3). Details of the X-ray structure determinations and refinements are provided in Table S-B3 (Supporting Information). Graphics were drawn with DIAMOND (Version 4.4).[90] The structural data for this paper have been deposited with the Cambridge Crystallographic Data Center (CCDC-numbers 1589564−1589571). These data can be obtained free of charge via www.ccdc.cam.ac.uk/data_request/cif.

Computational Section. Conformational searches and preliminary DFT calculations were run with Spartan'16 (Irvine, CA, 2017) using default grids and convergence criteria. DFT and TDDFT calculations were run with the Gaussian suite,[91] using default grids and convergence criteria. The X-ray structure of Λ-(*R*)-**1** was used as starting geometry, and the structure of Δ-(*R*)-**1** was built thereof. First, a conformational search was run on Λ-(*R*)-**1** and Δ-(*R*)-**1** with molecular mechanics (Merck Molecular force field, MMFF) using the Monte Carlo algorithm implemented in Spartan'16. All structures thus found were preoptimized with DFT at the B3LYP/6-31G(d) level in Spartan'16. DFT geometry optimizations were run in Gaussian with three different combinations of functionals and basis sets: B3LYP with 6-31G(d) on C, N, O, and H, and TZV on Co (henceforth indicated as "mixed" base); same as above, with D3BJ dispersion correction;[73] M06 with def2-SVP on all atoms, either in vacuo or using the IEF-PCM solvent model for chloroform.[92] A relatively small number of conformers was found with both functionals (see Tables S-D1 and S-D2, Supporting Information). According to M06/def2-SVP (either in vacuo or with PCM) and B3LYP-D3BJ/mixed calculations, the Λ-(*R*) diastereomer is more stable than the Δ-(*R*) one, while the opposite result was found by B3LYP/mixed calculations. This discrepancy highlights the inherent difficulty of a correct prediction of the diastereomeric population if relying only on a computational approach. TDDFT calculations were run on all relevant DFT minima with several functionals: B3LYP,[74,75] PBE0,[93] CAM-B3LYP,[94] ωB97X-D,[95] M06,[76] M06-L,[76] and M11-L.[96] They were used in combination with def2-SVP and def2-TZVP basis sets[77] (on all atoms). The calculations included 80 to 120 excited states (roots), depending on the functional. All calculations were run in vacuo, except for some test calculations, which included the polarizable continuum solvent model (PCM) for chloroform and gave results consistent with vacuum. Component spectra were averaged according to the Boltzmann distribution at 300 K using the M06/def2-SVP populations for the conformers with both Λ and Δ chirality-at-metal; an overall population of 20% was assigned to the set of conformers with Δ chirality, based on VT experiments (otherwise their contribution would be negligible). Frequency calculations (providing IR and VCD spectra) were run at B3LYP/def2-TZVP level, using geometries optimized at the same level, and the averaging approach described above. Absorption, ECD, IR, and VCD spectra were averaged and plotted using the software SpecDis (v 1.71).[97,98] Kohn−Sham orbitals and transition densities were plotted with the software MultiWfn (v 3.4).[99]

■ ASSOCIATED CONTENT

Supporting Information

The Supporting Information is available free of charge on the ACS Publications website at DOI: 10.1021/acs.inorgchem.8b01932.

Synthetic details and characterization data; X-ray data; additional CD data; additional computational data (PDF)

Accession Codes

CCDC 1589564−1589571 contain the supplementary crystallographic data for this paper. These data can be obtained free of charge via www.ccdc.cam.ac.uk/data_request/cif, or by emailing data_request@ccdc.cam.ac.uk, or by contacting The Cambridge Crystallographic Data Centre, 12 Union Road, Cambridge CB2 1EZ, UK; fax: +44 1223 336033.

■ AUTHOR INFORMATION

Corresponding Authors

*E-mail: gennaro.pescitelli@unipi.it (G.P.).
*E-mail: steffen.luedeke@pharmazie.uni-freiburg.de (S.L.).
*E-mail: enamullah@juniv.edu (M.E.).
*E-mail: janiak@uni-duesseldorf.de. (C.J.).

ORCID

Gennaro Pescitelli: 0000-0002-0869-5076
Steffen Lüdeke: 0000-0003-1498-5552
Lorenzo Di Bari: 0000-0003-2347-2150
Mohammed Enamullah: 0000-0002-6905-3210
Christoph Janiak: 0000-0002-6288-9605

Notes

The authors declare no competing financial interest.

■ ACKNOWLEDGMENTS

We acknowledge the "Wazed Miah Science Research Centre" at Jahangirnagar University, Dhaka, Bangladesh, for obtaining CV, variable-temperature ^{1}H NMR spectra, and elemental data. Francesco Zinna is gratefully acknowledged for assistance in NIR-CD measurements. We thank Klaus Ditrich (ChiPros) at BASF SE, Ludwigshafen, for providing the enantiopure *N*-(aryl) ethylamines. M.G. gives thanks for the support from the Polish Ministry of Science and Higher Education ("Mobilnosc Plus" grant no. 1286/MOB/IV/2015/0). Some Gaussian computations were performed at Wroclaw Centre for Networking and Supercomputing (WCSS) in Poland.

■ REFERENCES

(1) Amouri, H.; Gruselle, M. *Chirality in Transition Metal Chemistry: Molecules, Supramolecular Assemblies and Materials*; John Wiley & Sons: Chichester, UK, 2008.

DOI: 10.1021/acs.inorgchem.8b01932
Inorg. Chem. 2018, 57, 13397−13408

(2) Ma, W.; Xu, L.; de Moura, A. F.; Wu, X.; Kuang, H.; Xu, C.; Kotov, N. A. Chiral Inorganic Nanostructures. *Chem. Rev.* **2017**, *117*, 8041−8093.
(3) Brunner, H. Optically active organometallic compounds of transition elements with chiral metal atoms. *Angew. Chem., Int. Ed.* **1999**, *38*, 1194−1208.
(4) Zhang, L.; Meggers, E. Stereogenic-Only-at-Metal Asymmetric Catalysts. *Chem. - Asian J.* **2017**, *12*, 2335−2342.
(5) Yan, Z.-H.; Li, D.; Yin, X.-B. Review for chiral-at-metal complexes and metal-organic framework enantiomorphs. *Sci. Bull.* **2017**, *62*, 1344−1354.
(6) Wang, C.; Chen, L.-A.; Huo, H.; Shen, X.; Harms, K.; Gong, L.; Meggers, E. Asymmetric Lewis acid catalysis directed by octahedral rhodium centrochirality. *Chem. Sci.* **2015**, *6*, 1094−1100.
(7) Knof, U.; von Zelewsky, A. Predetermined Chirality at Metal Centers. *Angew. Chem., Int. Ed.* **1999**, *38*, 302−322.
(8) Janiak, C. Engineering coordination polymers towards applications. *Dalton Trans.* **2003**, 2781−2804.
(9) Crassous, J. Transfer of chirality from ligands to metal centers: recent examples. *Chem. Commun.* **2012**, *48*, 9684−9692.
(10) Miyake, H.; Tsukube, H. Coordination chemistry strategies for dynamic helicates: time-programmable chirality switching with labile and inert metal helicates. *Chem. Soc. Rev.* **2012**, *41*, 6977−6991.
(11) Zhang, L.; Meggers, E. Steering Asymmetric Lewis Acid Catalysis Exclusively with Octahedral Metal-Centered Chirality. *Acc. Chem. Res.* **2017**, *50*, 320−330.
(12) Wu, T.; You, X.-Z.; Bouř, P. Applications of chiroptical spectroscopy to coordination compounds. *Coord. Chem. Rev.* **2015**, *284*, 1−18.
(13) Polavarapu, P. L. *Chiroptical Spectroscopy: Fundamentals and Applications*; CRC Press: Boca Raton, FL, 2016.
(14) Fan, Z.; Govorov, A. O. Plasmonic Circular Dichroism of Chiral Metal Nanoparticle Assemblies. *Nano Lett.* **2010**, *10*, 2580−2587.
(15) Kuzyk, A.; Schreiber, R.; Fan, Z.; Pardatscher, G.; Roller, E.-M.; Hoegele, A.; Simmel, F. C.; Govorov, A. O.; Liedl, T. DNA-based self-assembly of chiral plasmonic nanostructures with tailored optical response. *Nature* **2012**, *483*, 311−314.
(16) Kotova, O.; Blasco, S.; Twamley, B.; O'Brien, J.; Peacock, R. D.; Kitchen, J. A.; Martinez-Calvo, M.; Gunnlaugsson, T. The application of chiroptical spectroscopy (circular dichroism) in quantifying binding events in lanthanide directed synthesis of chiral luminescent self-assembly structures. *Chem. Sci.* **2015**, *6*, 457−471.
(17) Zinna, F.; Giovanella, U.; Di Bari, L. Highly Circularly Polarized Electroluminescence from a Chiral Europium Complex. *Adv. Mater.* **2015**, *27*, 1791−1795.
(18) Domingo, N.; Bellido, E.; Ruiz-Molina, D. Advances on structuring, integration and magnetic characterization of molecular nanomagnets on surfaces and devices. *Chem. Soc. Rev.* **2012**, *41*, 258−302.
(19) Domingos, S. R.; Hartl, F.; Buma, W. J.; Woutersen, S. Elucidating the Structure of Chiral Molecules by using Amplified Vibrational Circular Dichroism: From Theory to Experimental Realization. *ChemPhysChem* **2015**, *16*, 3363−3373.
(20) Nafie, L. A. *Vibrational Optical Activity. Principles and Applications*; John Wiley & Sons: Chichester, UK, 2011.
(21) Domingos, S. R.; Sanders, H. J.; Hartl, F.; Buma, W. J.; Woutersen, S. Switchable Amplification of Vibrational Circular Dichroism as a Probe of Local Chiral Structure. *Angew. Chem., Int. Ed.* **2014**, *53*, 14042−14045.
(22) Domingos, S. R.; Huerta-Viga, A.; Baij, L.; Amirjalayer, S.; Dunnebier, D. A. E.; Walters, A. J. C.; Finger, M.; Nafie, L. A.; de Bruin, B.; Buma, W. J.; Woutersen, S. Amplified Vibrational Circular Dichroism as a Probe of Local Biomolecular Structure. *J. Am. Chem. Soc.* **2014**, *136*, 3530−3535.
(23) Berardozzi, R.; Badetti, E.; Carmo dos Santos, N. A.; Wurst, K.; Licini, G.; Pescitelli, G.; Zonta, C.; Di Bari, L. Co(II)-induced giant vibrational CD provides a new design of methods for rapid and sensitive chirality recognition. *Chem. Commun.* **2016**, *52*, 8428−8431.
(24) Arrico, L.; Angelici, G.; Di Bari, L. Taking advantage of Co(II) induced enhanced VCD for the fast and sensitive determination of enantiomeric excess. *Org. Biomol. Chem.* **2017**, *15*, 9800−9803.
(25) Carmo Dos Santos, N. A.; Badetti, E.; Licini, G.; Abbate, S.; Longhi, G.; Zonta, C. A stereodynamic fluorescent probe for amino acids. Circular dichroism and circularly polarized luminescence analysis. *Chirality* **2018**, *30*, 65−73.
(26) Sakiyama, H.; Okawa, H.; Matsumoto, N.; Kida, S. Stereoselectivity in Diastereomeric Tetrahedral Metal(II) Complexes of Chiral Salicylideneamines: Crystal Structure and Molecular Mechanics Calculation of Bis[N-(l-menthyl)salicylideneaminato]cobalt(II). *Bull. Chem. Soc. Jpn.* **1991**, *64*, 2644−2647.
(27) Chamayou, A. C.; Lüdeke, S.; Brecht, V.; Freedman, T. B.; Nafie, L. A.; Janiak, C. Chirality and Diastereoselection of Δ/Λ-Configured Tetrahedral Zinc Complexes through Enantiopure Schiff Base Complexes: Combined Vibrational Circular Dichroism, Density Functional Theory, ^{1}H-NMR, and X-ray Structural Studies. *Inorg. Chem.* **2011**, *50*, 11363−11374.
(28) Chamayou, A. C.; Makhloufi, G.; Nafie, L. A.; Janiak, C.; Lüdeke, S. Solvation-Induced Helicity Inversion of Pseudotetrahedral Chiral Copper(II) Complexes. *Inorg. Chem.* **2015**, *54*, 2193−2203.
(29) Enamullah, M.; Makhloufi, G.; Ahmed, R.; Joy, B. A.; Islam, M. A.; Padula, D.; Hunter, H.; Pescitelli, G.; Janiak, C. Synthesis, X-ray, and Spectroscopic Study of Dissymmetric Tetrahedral Zinc(II) Complexes from Chiral Schiff Base Naphthaldiminate Ligands with Apparent Exception to the ECD Exciton Chirality. *Inorg. Chem.* **2016**, *55*, 6449−6464.
(30) Enamullah, M.; Quddus, M. A.; Hasan, M. R.; Pescitelli, G.; Berardozzi, R.; Makhloufi, G.; Vasylyeva, V.; Janiak, C. Chirality at metal and helical ligand folding in optical isomers of chiral bis(naphthaldiminato)nickel(II) complexes. *Dalton Trans.* **2016**, *45*, 667−680.
(31) Enamullah, M.; Quddus, M. A.; Hasan, M. R.; Pescitelli, G.; Berardozzi, R.; Reiss, G. J.; Janiak, C. Syntheses, Spectroscopy, and Structural Analyses of Dinuclear Chiral-at-Metal -Aqua-tetrakis (R or S)-N-1-(Ar)ethylsalicylaldiminato di-L- or -D-nickel(II) Complexes. *Eur. J. Inorg. Chem.* **2015**, *2015*, 2758−2768.
(32) Enamullah, M.; Uddin, A.; Pescitelli, G.; Berardozzi, R.; Makhloufi, G.; Vasylyeva, V.; Chamayou, A. C.; Janiak, C. Induced chirality-at-metal and diastereoselectivity at Δ/Λ-configured distorted square-planar copper complexes by enantiopure Schiff base ligands: combined circular dichroism, DFT and X-ray structural studies. *Dalton Trans.* **2014**, *43*, 3313−3329.
(33) Enamullah, M.; Vasylyeva, V.; Janiak, C. Chirality and diastereoselection of Δ/Λ-configured tetrahedral zinc(II) complexes with enantiopure or racemic Schiff base ligands. *Inorg. Chim. Acta* **2013**, *408*, 109−119.
(34) von Zelewsky, A. *Stereochemistry of Coordination Compounds*; Wiley: Chichester, UK, 1996.
(35) Di Bari, L.; Salvadori, P. Solution structure of chiral lanthanide complexes. *Coord. Chem. Rev.* **2005**, *249*, 2854−2879.
(36) He, Y. N.; Cao, X. L.; Nafie, L. A.; Freedman, T. B. Ab initio VCD calculation of a transition-metal containing molecule and a new intensity enhancement mechanism for VCD. *J. Am. Chem. Soc.* **2001**, *123*, 11320−11321.
(37) Holm, R. H.; Kennepohl, P.; Solomon, E. I. Structural and Functional Aspects of Metal Sites in Biology. *Chem. Rev.* **1996**, *96*, 2239−2314.
(38) Che, C.-M.; Huang, J.-S. Metal complexes of chiral binaphthyl Schiff-base ligands and their application in stereoselective organic transformations. *Coord. Chem. Rev.* **2003**, *242*, 97−113.
(39) Ma, L.-F.; Wang, L.-Y.; Lu, D.-H.; Batten, S. R.; Wang, J.-G. Structural Variation from 1D to 3D: Effects of Temperature and pH Value on the Construction of Co(II)-H_2tbip/bpp Mixed Ligands System. *Cryst. Growth Des.* **2009**, *9*, 1741−1749.
(40) Kobayashi, M.; Shimizu, S. Cobalt proteins. *Eur. J. Biochem.* **1999**, *261*, 1−9.
(41) Gorecki, M.; Carpita, L.; Arrico, L.; Zinna, F.; Di Bari, L. Chiroptical methods in a wide wavelength range for obtaining Ln^{3+}

DOI: 10.1021/acs.inorgchem.8b01932
Inorg. Chem. 2018, 57, 13397−13408

complexes with circularly polarized luminescence of practical interest. *Dalton Trans.* **2018**, *47*, 7166−7177.
(42) Di Pietro, S.; Lo Piano, S.; Di Bari, L. Pseudocontact shifts in lanthanide complexes with variable crystal field parameters. *Coord. Chem. Rev.* **2011**, *255*, 2810−2820.
(43) Sakiyama, H.; Ōkawa, H.; Matsumoto, N.; Kida, S. A tetrahedral zinc(II) complex of N-(R)-1-phenylethylsalicylideneimine. Structural and circular dichroism spectral investigations on stereoselectivity. *J. Chem. Soc., Dalton Trans.* **1990**, 2935−2939.
(44) Evans, D. F. The determination of the paramagnetic susceptibility of substances in solution by nuclear magnetic resonance. *J. Chem. Soc.* **1959**, 2003−2005.
(45) Linert, W.; Enamullah, M.; Gutmann, V.; Jameson, R. F. Spin-crossover complexes in solution. III. Substituent- and solvent effects on the spin-equilibrium of 4-substituted iron(II)-2,6-bis-(benzimidazol-2′-yl)-pyridine systems. *Monatsh. Chem.* **1994**, *125*, 661−670.
(46) Enamullah, M.; Linert, W. Spin-crossover of $[Fe(Cl\text{-}bzimpy)_2](ClO_4)_2$ iduced by deprotonation. *J. Coord. Chem.* **1995**, *35*, 325−335.
(47) Enamullah, M. Studies of the spin crossover complex iron(II)-2,6-bis-(benzimidazol-2 ′-yl)pyridine in propanediol-1,2-carbonate. *J. Coord. Chem.* **1997**, *42*, 231−239.
(48) Enamullah, M.; Linert, W. Synthesis and characterization of spin-free [Co-2(N,N ′-tetra(4-antipyrylmethyl)-1,2-diaminoethane)Cl-4]. *Monatsh. Chem.* **1998**, *129*, 3−7.
(49) Enamullah, M.; Hasegawa, M.; Fukuda, Y.; Linert, W.; Hoshi, T. Synthesis, characterization and spin-crossover behaviors of [Co-(hydroxycarboxylato)(triphos)] complexes. *Bull. Chem. Soc. Jpn.* **2002**, *75*, 2449−2453.
(50) Enamullah, M. Synthetic and spectroscopic characterization of $[Co(triphos)(chiral\ amino\ alcoholato)](BPh_4)$ complexes. *J. Coord. Chem.* **2010**, *63*, 643−651.
(51) Orchard, A. F. *Magnetochemistry*; Oxford University Press: Oxford, 2003.
(52) Sakiyama, H.; Okawa, H.; Oguni, N.; Katsuki, T.; Irie, R. CD Spectral Diagnosis of Absolute Configuration of Tetrahedral or Pseudo-Tetrahedral Metal Complexes of Salicylideneiminates. *Bull. Chem. Soc. Jpn.* **1992**, *65*, 606−608.
(53) Ziegler, M.; von Zelewsky, A. Charge-transfer excited state properties of chiral transition metal coordination compounds studied by chiroptical spectroscopy. *Coord. Chem. Rev.* **1998**, *177*, 257−300.
(54) Bosnich, B. An interpretation of the circular dichroism and electronic spectra of salicylaldimine complexes of square-coplanar diamagnetic nickel(II). *J. Am. Chem. Soc.* **1968**, *90*, 627−632.
(55) Cotton, F. A.; Wilkinson, G.; Murillo, C. A.; Bochmann, M. *Advanced Inorganic Chemistry*, 6th ed.; John Wiley & Sons: New York, 1999.
(56) Mason, S. F. *Molecular optical activity and the chiral discriminations*; Cambridge University Press: Cambridge, 1982.
(57) Thulstrup, P. W.; Broge, L.; Larsen, E.; Springborg, J. On the electronic structure and spectroscopic properties of a pseudo-tetrahedral cationic cobalt(II) tetraamine complex - ([35]-adamanzane)cobalt(II). *Dalton Trans.* **2003**, 3199−3204.
(58) Barnett, C. J.; Drake, A. F.; Kuroda, R.; Mason, S. F.; Savage, S. Vibrational Electronic Interaction in the Infrared Circular-Dichroism Spectra of Transition-Metal Complexes. *Chem. Phys. Lett.* **1980**, *70*, 8−10.
(59) Johannessen, C.; Thulstrup, P. W. Vibrational circular dichroism spectroscopy of a spin-triplet bis-(biuretato) cobaltate(III) coordination compound with low-lying electronic transitions. *Dalton Trans.* **2007**, 1028−1033.
(60) Merten, C.; Hiller, K.; Xu, Y. J. Effects of electron configuration and coordination number on the vibrational circular dichroism spectra of metal complexes of trans-1,2-diaminocyclohexane. *Phys. Chem. Chem. Phys.* **2012**, *14*, 12884−12891.
(61) Sato, H.; Mori, Y.; Fukuda, Y.; Yamagishi, A. Syntheses and Vibrational Circular Dichroism Spectra of the Complete Series of $[Ru((-)\text{- or }(+)\text{-tfac})_n(acac)_{3-n}]$ (n = 0−3, tfac = 3-Trifluoroacetyl-camphorato and acac = Acetylacetonato). *Inorg. Chem.* **2009**, *48*, 4354−4361.
(62) Sato, H.; Taniguchi, T.; Nakahashi, A.; Monde, K.; Yamagishi, A. Effects of central metal ions on vibrational circular dichroism spectra of Tris-(beta-diketonato)metal(III) complexes. *Inorg. Chem.* **2007**, *46*, 6755−6766.
(63) Young, D. A.; Freedman, T. B.; Lipp, E. D.; Nafie, L. A. Vibrational Circular-Dichroism in Transition-Metal Complexes 0.2. Ion Association, Ring Conformation, and Ring Currents of Ethylenediamine Ligands. *J. Am. Chem. Soc.* **1986**, *108*, 7255−7263.
(64) Lo Piano, S.; Di Pietro, S.; Di Bari, L. Shape-conserving enhancement of vibrational circular dichroism in lanthanide complexes. *Chem. Commun.* **2012**, *48*, 11996−11998.
(65) Nafie, L. A. Theory of vibrational circular dichroism and infrared absorption: Extension to molecules with low-lying excited electronic states. *J. Phys. Chem. A* **2004**, *108*, 7222−7231.
(66) Srebro-Hooper, M.; Autschbach, J. Calculating Natural Optical Activity of Molecules from First Principles. *Annu. Rev. Phys. Chem.* **2017**, *68*, 399−420.
(67) Autschbach, J.; Nitsch-Velasquez, L.; Rudolph, M. Time-Dependent Density Functional Response Theory for Electronic Chiroptical Properties of Chiral Molecules. *Top. Curr. Chem.* **2010**, *298*, 1−98.
(68) Vargas, A.; Zerara, M.; Krausz, E.; Hauser, A.; Lawson Daku, L. M. Density-Functional Theory Investigation of the Geometric, Energetic, and Optical Properties of the Cobalt(II)tris(2,2′-bipyridine) Complex in the High-Spin and the Jahn−Teller Active Low-Spin States. *J. Chem. Theory Comput.* **2006**, *2*, 1342−1359.
(69) Autschbach, J. Calculating Electronic Optical Activity of Coordination Compounds. In *Comprehensive Inorganic Chemistry II*, 2nd ed.; Reedijk, J., Poeppelmeier, K., Eds.; Elsevier: Amsterdam, 2013; pp 407−426.
(70) Leticia, G.; Daniel, E.; Luis, S. A. Progress and Challenges in the Calculation of Electronic Excited States. *ChemPhysChem* **2012**, *13*, 28−51.
(71) Ipatov, A.; Cordova, F.; Doriol, L. J.; Casida, M. E. Excited-state spin-contamination in time-dependent density-functional theory for molecules with open-shell ground states. *J. Mol. Struct.: THEOCHEM* **2009**, *914*, 60−73.
(72) Casida, M. E.; Jamorski, C.; Casida, K. C.; Salahub, D. R. Molecular excitation energies to high-lying bound states from time-dependent density-functional response theory: Characterization and correction of the time-dependent local density approximation ionization threshold. *J. Chem. Phys.* **1998**, *108*, 4439−4449.
(73) Grimme, S.; Ehrlich, S.; Goerigk, L. Effect of the damping function in dispersion corrected density functional theory. *J. Comput. Chem.* **2011**, *32*, 1456−1465.
(74) Becke, A. D. Density-functional thermochemistry. III. The role of exact exchange. *J. Chem. Phys.* **1993**, *98*, 5648−5652.
(75) Vosko, S. H.; Wilk, L.; Nusair, M. Accurate spin-dependent electron liquid correlation energies for local spin density calculations: a critical analysis. *Can. J. Phys.* **1980**, *58*, 1200−1211.
(76) Zhao, Y.; Truhlar, D. G. The M06 suite of density functionals for main group thermochemistry, thermochemical kinetics, noncovalent interactions, excited states, and transition elements: two new functionals and systematic testing of four M06 functionals and 12 other functionals. *Theor. Chem. Acc.* **2008**, *119*, 525−525.
(77) Weigend, F.; Ahlrichs, R. Balanced basis sets of split valence, triple zeta valence and quadruple zeta valence quality for H to Rn: Design and assessment of accuracy. *Phys. Chem. Chem. Phys.* **2005**, *7*, 3297−3305.
(78) Jacquemin, D.; Perpète, E. A.; Scuseria, G. E.; Ciofini, I.; Adamo, C. TD-DFT Performance for the Visible Absorption Spectra of Organic Dyes: Conventional versus Long-Range Hybrids. *J. Chem. Theory Comput.* **2008**, *4*, 123−135.
(79) Mai, S.; Plasser, F.; Dorn, J.; Fumanal, M.; Daniel, C.; González, L. Quantitative wave function analysis for excited states of transition metal complexes. *Coord. Chem. Rev.* **2018**, *361*, 74−97.
(80) Cotton, F. A.; Goodgame, D. M. L.; Goodgame, M. The Electronic Structures of Tetrahedral Cobalt(II) Complexes. *J. Am. Chem. Soc.* **1961**, *83*, 4690−4699.

DOI: 10.1021/acs.inorgchem.8b01932
Inorg. Chem. 2018, 57, 13397−13408

(81) Freedman, T. B.; Young, D. A.; Oboodi, M. R.; Nafie, L. A. Vibrational Circular-Dichroism in Transition-Metal Complexes 0.3. Ring Currents and Ring Conformations of Amino-Acid Ligands. *J. Am. Chem. Soc.* **1987**, *109*, 1551−1559.
(82) Li, X.; Dai, J.-W.; Wang, H.-X.; Wu, A.-A.; Zhou, Z.-H. Chiral and achiral vanadyl lactates with vibrational circular dichroism: Toward the chiral metal cluster in nitrogenase. *Inorg. Chim. Acta* **2016**, *453*, 501−506.
(83) Wu, C. L.; Hudecová, J.; You, X. Z.; Urbanová, M.; Bouř, P. Comparison of the Electronic and Vibrational Optical Activity of a Europium(III) Complex. *Chem. - Eur. J.* **2015**, *21*, 5807−5813.
(84) Raiford, D. S.; Fisk, C. L.; Becker, E. D. Calibration of Methanol and Ethylene-Glycol Nuclear Magnetic-Resonance Thermometers. *Anal. Chem.* **1979**, *51*, 2050−2051.
(85) König, E. Magnetische Eigenschaften der Koordinations- und Metallorganischen Verbindungen der Übergangselemente. In *Landolt-Börnstein, Zahlenwerte und Funktionen aus Naturwissenschaften und Technik*; Springer-Verlag: Berlin, Göttingen, Heidelberg, 1966.
(86) *APEX2, data collection program for the CCD area-detector system*, Version 2.1-0; Bruker Analytical X-ray Systems: Madison, WI, 2006.
(87) *SAINT, data reduction and frame integration program for the CCD area-detector system*; Bruker Analytical X-ray Systems: Madison, WI, 2006.
(88) Sheldrick, G. A short history of SHELX. *Acta Crystallogr., Sect. A: Found. Crystallogr.* **2008**, *64*, 112−122.
(89) Sheldrick, G. M. *Program SADABS*; University of Göttingen: Göttingen, Germany, 1996.
(90) Brandenburg, K. *Diamond (Version 3.2), Crystal and Molecular Structure Visualization*; Crystal Impact − K. Brandenburg & H. Putz Gbr: Bonn, Germany, 2009.
(91) Frisch, M. J.; Trucks, G. W.; Schlegel, H. B.; Scuseria, G. E.; Robb, M. A.; Cheeseman, J. R.; Scalmani, G.; Barone, V.; Petersson, G. A.; Nakatsuji, H.; Li, X.; Caricato, M.; Marenich, A. V.; Bloino, J.; Janesko, B. G.; Gomperts, R.; Mennucci, B.; Hratchian, H. P.; Ortiz, J. V.; Izmaylov, A. F.; Sonnemberg, J. L.; Williams-Young, D.; Ding, F.; LIpparini, F.; Egidi, F.; Goings, J.; Peng, B.; Petrone, A.; Henderson, T.; Ranasinghe, D.; Zakrzewski, V. G.; Gao, J.; Rega, N.; Zheng, G.; Liang, W.; Hada, M.; Ehara, M.; Toyota, K.; Fukuda, R.; Hasegawa, J.; Ishida, M.; Nakajima, T.; Honda, Y.; Kitao, O.; Nakai, H.; Vreven, T.; Throssell, K.; Montgomery, J. J. A.; Peralta, J. E.; Ogliaro, F.; Bearpark, M.; Heyd, J. J.; Brothers, E.; Kudin, K. N.; Staroverov, V. N.; Keith, T. A.; Kobayashi, R.; Normand, J.; Raghavachari, K.; Rendell, A.; Burant, J. C.; Iyengar, S. S.; Tomasi, J.; Cossi, M.; Millam, J. M.; Klene, M.; Adamo, C.; Cammi, R.; Ochterski, J. W.; Martin, R. L.; Morokuma, K.; Farkas, O.; Foresman, J. B.; Fox, D. J. *Gaussian 16*, Revision A.03; Gaussian, Inc.: Wallingford, CT, 2016.
(92) Tomasi, J.; Mennucci, B.; Cammi, R. Quantum Mechanical Continuum Solvation Models. *Chem. Rev.* **2005**, *105*, 2999−3094.
(93) Adamo, C.; Barone, V. Toward reliable density functional methods without adjustable parameters: The PBE0 model. *J. Chem. Phys.* **1999**, *110*, 6158−6170.
(94) Yanai, T.; Tew, D. P.; Handy, N. C. A new hybrid exchange−correlation functional using the Coulomb-attenuating method (CAM-B3LYP). *Chem. Phys. Lett.* **2004**, *393*, 51−57.
(95) Chai, J.-D.; Head-Gordon, M. Long-range corrected hybrid density functionals with damped atom-atom dispersion corrections. *Phys. Chem. Chem. Phys.* **2008**, *10*, 6615−6620.
(96) Peverati, R.; Truhlar, D. G. M11-L: A Local Density Functional That Provides Improved Accuracy for Electronic Structure Calculations in Chemistry and Physics. *J. Phys. Chem. Lett.* **2012**, *3*, 117−124.
(97) Bruhn, T.; Schaumlöffel, A.; Hemberger, Y.; Bringmann, G. SpecDis: Quantifying the Comparison of Calculated and Experimental Electronic Circular Dichroism Spectra. *Chirality* **2013**, *25*, 243−249.
(98) Bruhn, T.; Schaumlöffel, A.; Hemberger, Y.; Pescitelli, G. *SpecDis version 1.71*, Berlin, Germany, 2017; https://specdis-software.jimdo.com/.
(99) Lu, T.; Chen, F. Multiwfn: A multifunctional wavefunction analyzer. *J. Comput. Chem.* **2012**, *33*, 580−592.

DOI: 10.1021/acs.inorgchem.8b01932
Inorg. Chem. 2018, 57, 13397−13408